International Journal of Experimental Research and Review (IJERR)

ISSN: 2455-4855 (Online) ***Original Article***
Received: 2nd August, 2021; **Accepted:** 15th November, 2021; **Published:** 30th December, 2021
DOI: https://doi.org/10.52756/ijerr.2021.v26.002

Study of Densification Behavior of SiAlONs Using Dysprosium Containing Additive System

Sudipta Nath* and Utpal Madhu

Department of Mechanical Engineering, Swami Vivekananda Institute of Science & Technology, Kolkata, West Bengal, India

E-mail / Orcid ID: SN, chobikobi@gmail.com; **UM,** utpalmadhu@gmail.com, https://orcid.org/0000-0001-7178-7072

***Corresponding Author:** chobikobi@gmail.com

Abstract

SiAlON ceramics have complicated chemistry and should be considered a group of alloys with diverse characteristics. It is generated when silicon nitride (Si_3N_4), aluminium oxide (Al_2O_3) and aluminium nitride (AlN) react together. If sintering aids such as Dysprosium oxide are added to the initial composition, fully dense polycrystalline bodies can be produced through pressureless sintering. Inter-granular phase composition and structure may be modified by dopants and sintering conditions, which significantly impact the characteristics of SiAlON ceramics. The focus of this study was concentrated on the nature of densification and nature of the phases that appeared in SiAlON. It was found that the volume and density of all the specimens considerably reduced and enhanced, respectively owing to sintering at elevated temperatures. The XRD results showed various phases as per their relative intensities, which indicates densification will alter different properties, especially mechanical and thermal properties.

Keywords: Densification, dysprosium oxide, heat treatment, shrinkage analysis, SiAlON, XRD characterization.

Introduction

In the mid '60s with the developments of Si_3N_4, a new era based on ceramics began. This unique material exhibited a combination of high strength, appreciable chemical inertness and excellent thermal shock withstanding properties. But in handling this material, two major difficulties had to be overcome, i.e., insufficient densification behaviour and production of complex or intricate shaped parts (Jack, 1976). To solve those problems, reaction bonding and hot pressing methods were employed. However, issues related to designing intricate parts were not over yet. On the other hand, the material thus produced proved its superiority over the metal-super alloy system in comparison during the operation of two

ceramic gas turbine engines at elevated temperatures. While working under extreme thermal shock and high stress, a phenomenal change in its property was noted.

The layer of irremovable silica (present within the system) reacted with MgO (additive) which produces a glassy second phase material. This deteriorates the shock withstanding property of the ceramic material. From this deduction, it was clear to the scientists that rather than doing with pure Si_3N_4, which was always a two-phase material, a single-phase material can do better. Proper alloying and introduction of oxygen in the crystal lattice is essential to prepare a single-phase homogeneous material. It was discovered that two different phases (α and β) are present in the Si_3N_4 crystal. Nitriding silicon with molecular nitrogen resulted in the formation of the α phase, which had around one in every 30 nitrogen atoms replaced by oxygen in its structure (Ekstrom and Nygren, 1992). In the Si-O-N system, the existing Si_2N_2O is just as good as a ceramic like Si_3N_4. It is built up of Si-O-N tetrahedral and consists of parallel sheet lattice as Si-N atoms are joined by Si-O-Si bonds. It was also observed that in the α phase structure, oxygen atoms replaced a few nitrogen atoms without changing the original structure as per simple principles of silicate chemistry.

SiAlON ceramics are potential prospects for engineering applications, and they are used in immersion heater and burner tubes, ceramic bearing balls, thermocouple protection tubes, gas turbines, welding and brazing fixtures and pins etc. Due to their great toughness and hardness, α-β-SiAlON and Si_3N_4 ceramics are employed as cutting tool materials. Due to a combination of high hardness, strength, and toughness, α-β-SiAlON ceramics offer certain benefits over Si_3N_4 ceramics among these two classes of materials. The mechanical characteristics of SiAlON ceramics are known to be impacted by microstructure evolution, and the microstructure is influenced by varied sintering settings (Satet et al., 2006; Shibata et al., 2004; Ziegler et al., 2003; Li et al., 2001; Liu and Nasser, 1998). α' can be strengthened *in-situ* by combining β-SiAlON (β', solid solution based on β-Si_3N_4, $Si_{3-x}Al_xO_xN_{4-x}$) and SiAlON polytype phases (Cao et al., 1992).

Individual SiAlON phases have various grain morphologies and inherent characteristics. From the early research works on M-SiAlON regarding its nature of densification, it was observed that rare earth metal oxide plays a big role. In this study, Dysprosium was used as additive during the synthesis of Dy-SiAlON as it exhibits maximum rate of densification at lower temperature.

Materials and methods

High purity (>99.9% purity) Si_3N_4 (UBE Co. Ltd., Japan), AlN (Tokuyama Corp., Japan), Al_2O_3 (Alcoa A16-SG, Pittsburgh, USA),and Dy_2O_3 (MSE Supplies, Tucson, AZ 85711, USA) powders were collected. Four different samples with various compositions (mixtures of Si_3N_4, AlN, α-Al_2O_3 and Dy_2O_3 powders in different weight ratios) were made for the experiment *viz.*S1 (80.08% Si_3N_4 & 19.92% additives), S2 (78.96% Si_3N_4 & 21.04% additives), S3 (77.82% Si_3N_4 & 22.18% additives), and S4 (76.24% Si_3N_4 & 13.76% additives). Sintering of the specimens was performed at various temperatures (1290°C-1850°C). The experimental procedure is shown in the flow chart (Fig. 1).

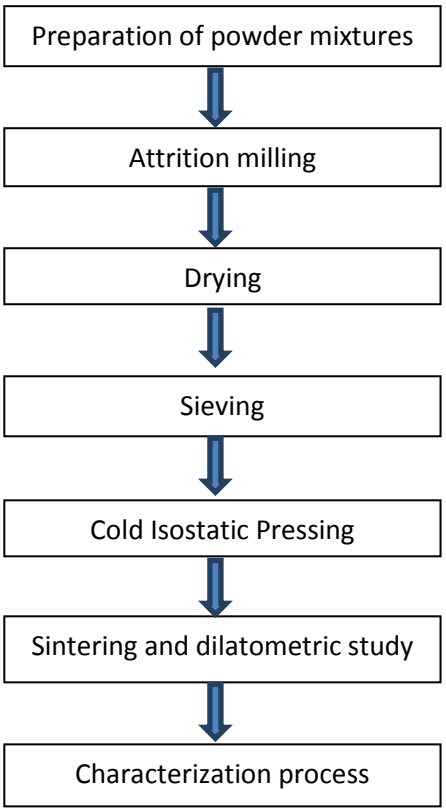

Fig. 1. Flow chart of the experiment.

Preparation of specimens

100 g of powder mixture for every particular batch were carefully transferred into SiAlON attritor jar. About 600 g of SiAlON balls were taken for attrition purposes depending on the composition of the mixture. Attrition milling was done in the Simens attritor milling system. Using SiAlON stirrer in acetone media powder mixtures were attrited for 3 hours @ 300 rpm. Once the attrition milling was over, the slurry was readily transferred to a flat, pre-washed dried steel tray and kept for 10 minutes for natural vaporization of acetone. To remove remaining acetone fume, a box dryer was used for several hours. The ball and powder mixture was sieved using 170 grit mesh to obtain uniform and fine grade particles. This procedure was repeated for every set of samples. Green pellets of the samples were made by using Cold Isostatic Press for heat treatment operation and Dilatometric study.

Green pellets of the samples were sintered at a temperature up to 1850°C @ 10°C/minute in a controlled atmosphere followed by rapid cooling. At the initial stage of sintering, Dilatometric studies were performed, and later densification studies were performed. During densification, Dilatometric studies were performed to observe actual shrinkage value and shrinkage rate. For the phase analysis operation, temperature zones were marked on the shrinkage rate curves, i.e., 1290°C, 1390°C, 1420°C, 1450°C, 1495°C and 1540°C. Heat treatment operations were performed at those temperature ranges along with fully sintered temperature, i.e., 1850°C for all samples. The phases of the heat-treated samples were identified by XRD analysis using

"SEIFERT 3000 P" diffractometer with CuK_{α} radiation.

Results and discussion

Weight, volume and density of green and sintered samples

It was noted that the volume and density of all the specimens significantly reduced and enhanced, respectively. The results are shown in Table 1. This phenomenon occurred due to the reduction of porosity of the samples due to the sintering process.

Shrinkage curve analysis

For samples S1-S4, there were no evidences of actual visible shrinkages up to 1200°C, 1225°C, 1255°C, and 1252°C, respectively. Around 1320°C, 1325°C, 1305°C, and 1327°C in the S1-S4 samples first small peak was shown on the SRC (shrinkage rate curve), respectively. It occurs due to the momentary expansions of the specimens. The expansions could be due to the formation of aluminates and DyAM ($Al_2Dy_4O_9$) within the system. After that, contractions and expansions were counterbalanced due to the formations of no. of intermediate phases within the systems of S1-S4 specimens at 1352°C, 1390°C, 1365°C, and 1375°C, respectively. Therefore, SRC displayed an almost flattened horizontal curve up to 1380°C, 1410°C, 1390°C, and 1397°C in all samples, respectively. Between 1380-1435°C, 1410-1435°C, 1415-1425°C, 1395°C-1425°C and there was a noticeable change in the SRC. These were the starting point of major shrinkage zones. At the temperature 1445°C (S1), 1445°C (S2), 1440°C (S3), and 1455°C (S4) ASC (actual shrinkage curve) started to move upward, which shows the beginning of actual shrinkage.

For the next 240 seconds, a steep curve was formed due to rapid shrinkage for specimen S1. For S2-S4, it was 240, 120, and 120 seconds, respectively. Up to 1455°C, the slope was almost linear for S1, S2, and S3 specimens, but for S4, the temperature was 1510°C. Shrinkage rate recorded for the samples during respective periods as 29.92µm/min, 24.56 µm/min, 29.63 µm/min, and 70.80 µm/min, respectively with actual shrinkage values of 0.13 mm, 0.09 mm, 0.08 mm, and 0.36 mm, respectively. Within next 368 seconds (S1), 360 seconds (S2), 360 seconds (S3), and 315 seconds (S4), sintering occurred vigorously and the SRC reached to its extreme value of 167.3 µm/min at 1557°C, 210.37 µm/min at 1527°C, 216.113 µm/min at 1551°C, and 345.57 µm/min at 1569°C, respectively. Actual shrinkages observed during this stage were 1.73 mm, 1.40 mm, 1.89 mm, and 2.01 mm, respectively, for S1-S4 samples. During this span, 90% of the total shrinkage occurred.

SRC falls rapidly in S1-S4 after 1562°C, 1530°C, 1560°C, and 1560°C, respectively and at 1595°C, 1585°C, 1595°C, and 1595°C, respectively it was creeping at a negligibly low rate. Two minor peaks were formed in all samples at 1650°C and 1730°C temperatures; although, ASC showed continuous shrinkages at a linear rate for all the samples. At the temperature of 1850°C total shrinkages were 3.0 mm (S1), 2.59 mm (S2), 2.40 mm (S3), and 2.99 mm (S4), respectively. Shrinkage curves are shown in Figures 2a-5b.

XRD analysis

In the samples S1-S4, it was observed from the XRD curves that several changes were taking place during sintering at different temperature ranges.

Table 1. Weight, volume and density of green and sintered samples.

Samples	Green sample			Sintered sample		
	Weight (g)	Volume (cc)	Density (g/cc)	Weight (g)	Volume (cc)	Density (g/cc)
S1	1.6994	1.0215	2.6634	1.6750	0.7846	3.2125
S2	2.3507	1.0526	2.4744	2.1096	0.8426	3.7628
S3	3.5263	1.7974	2.3200	3.3268	1.2991	3.4663
S4	1.6273	0.9086	2.4908	1.5574	0.7204	3.1618

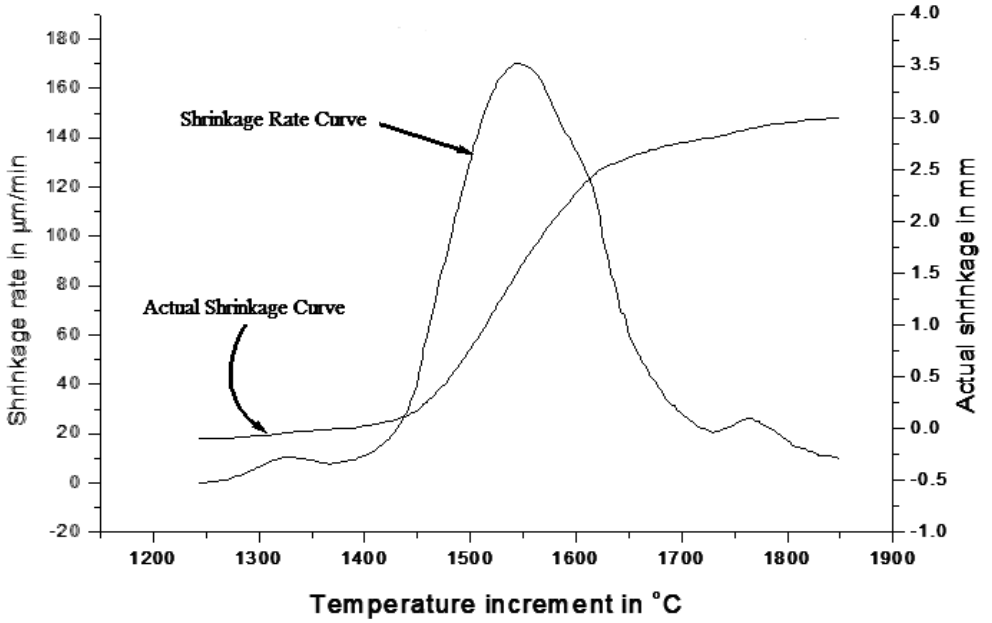

Fig. 2a. Shrinkage rate vs. temperature plot of specimen S1.

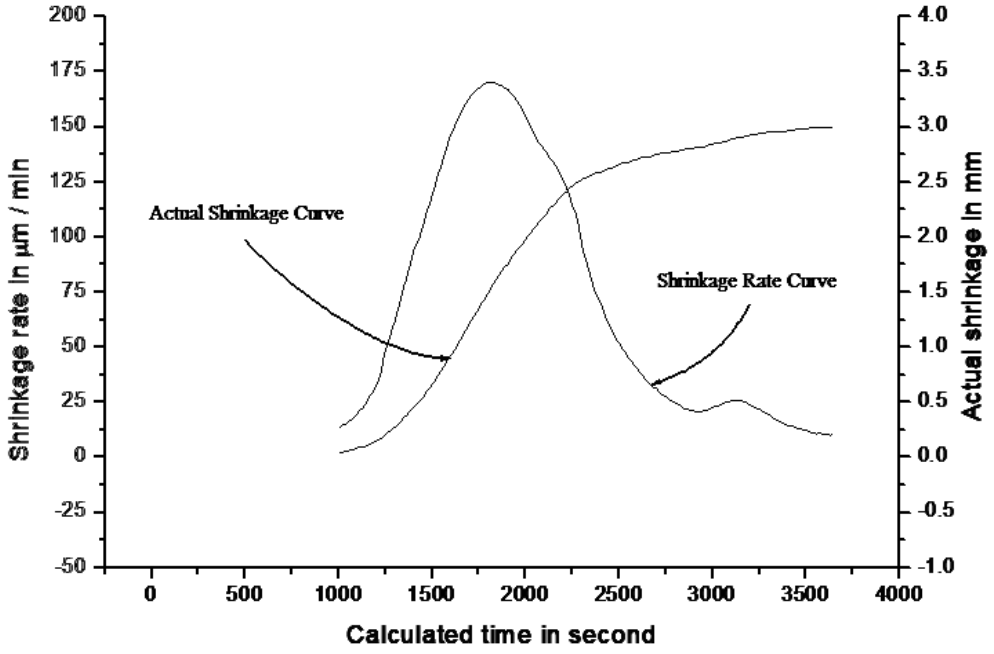

Fig. 2b. Shrinkage rate vs. time plot of specimen S1.

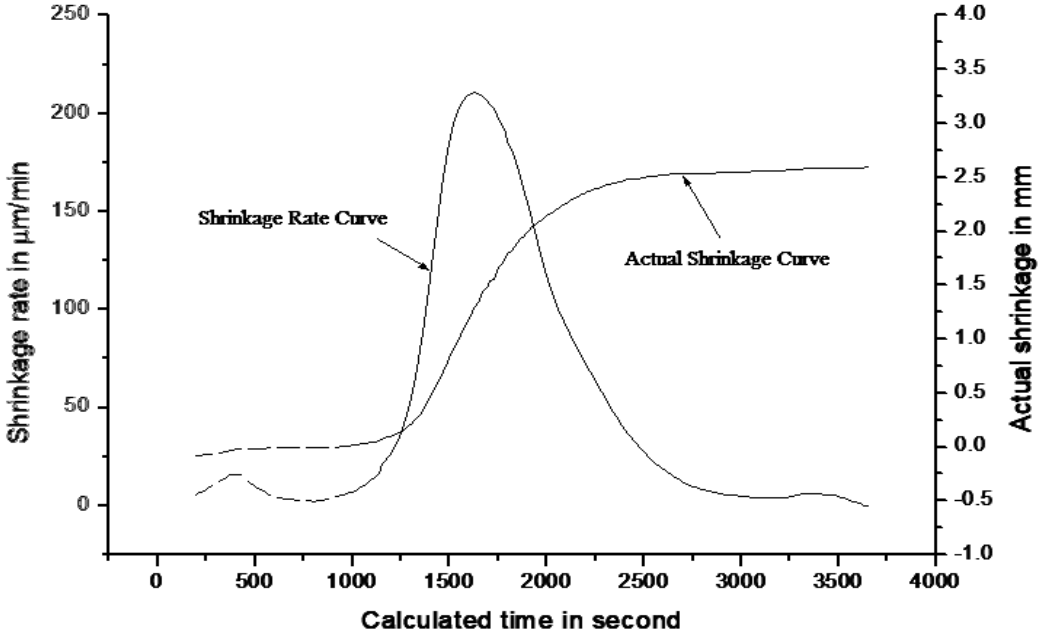

Fig. 3a. Shrinkage rate vs. temperature plot of specimen S2.

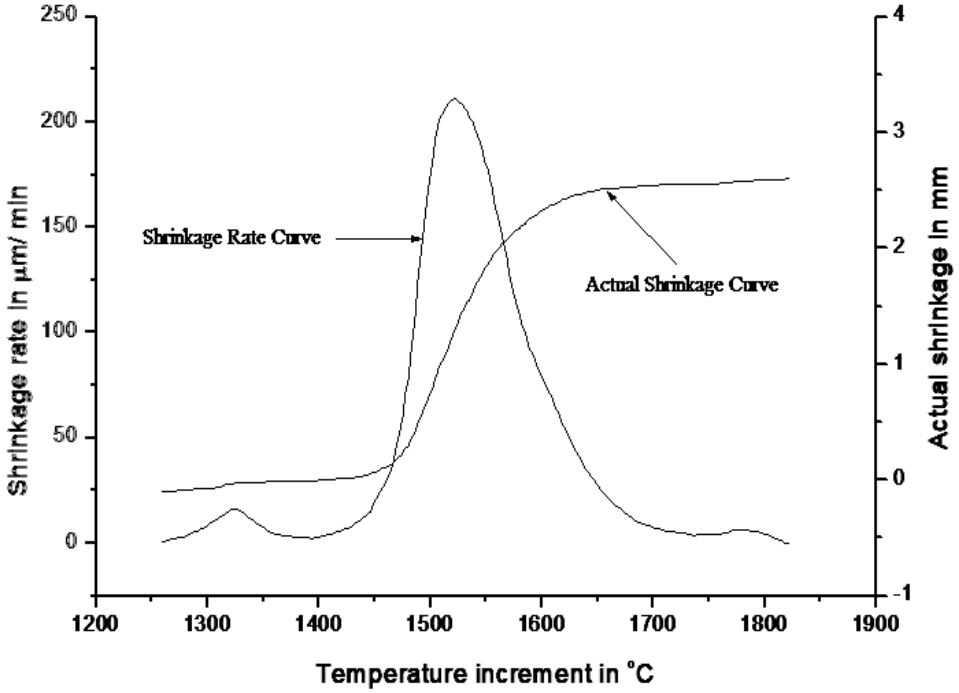

Fig. 3b. Shrinkage rate vs. time plot of specimen S2.

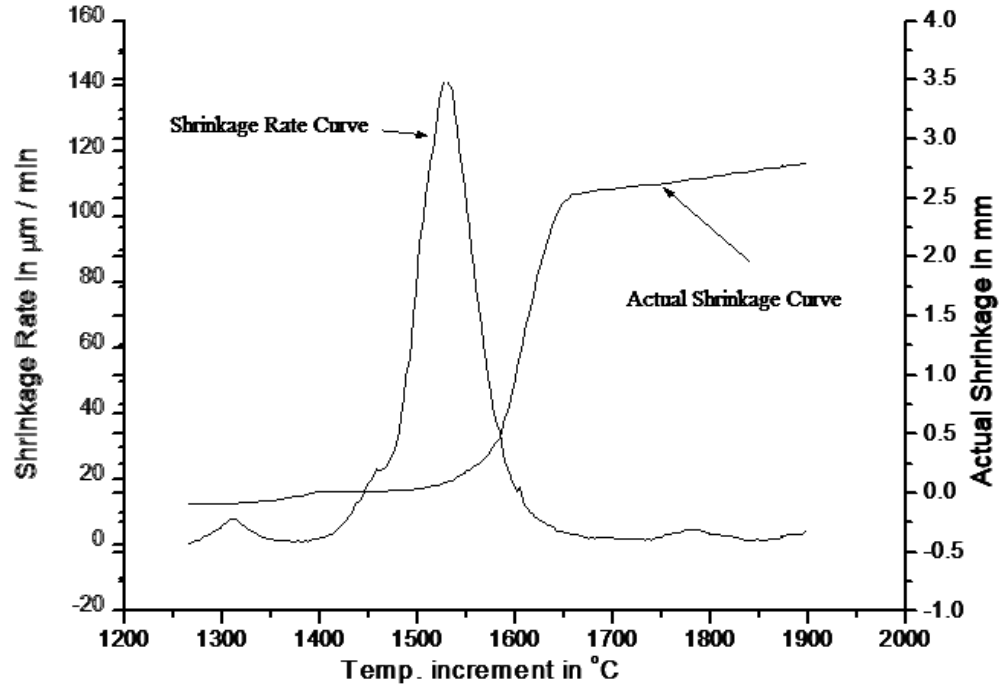

Fig. 4a. Shrinkage rate vs. temperature plot of specimen S3.

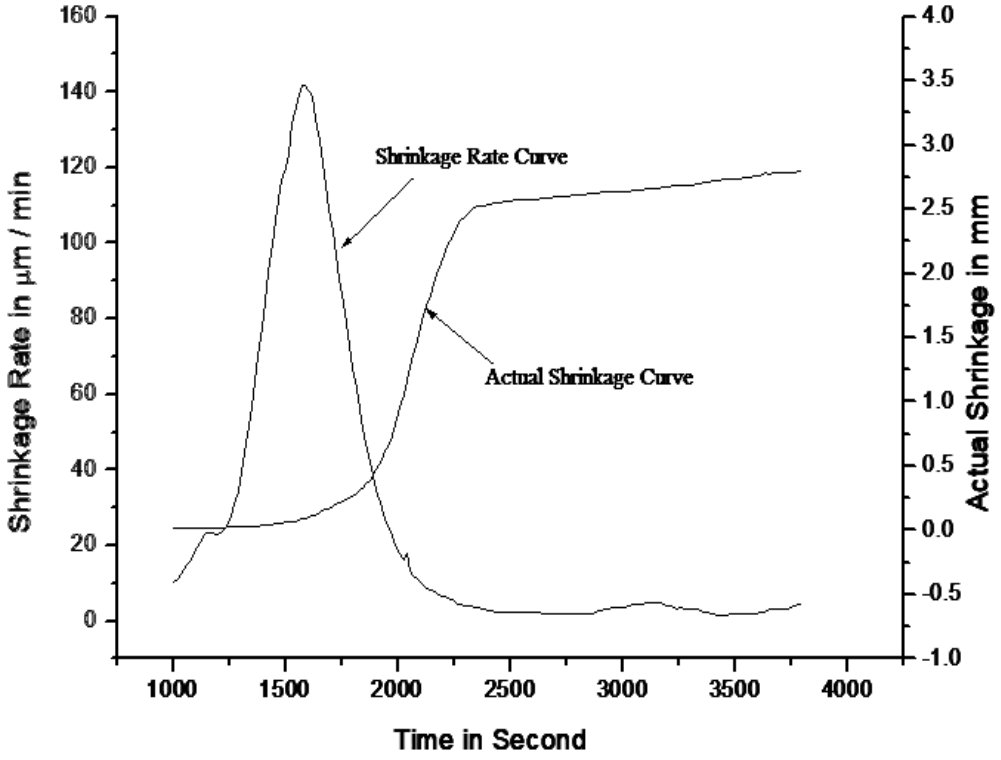

Fig. 4b. Shrinkage rate vs. time plot of specimen S3.

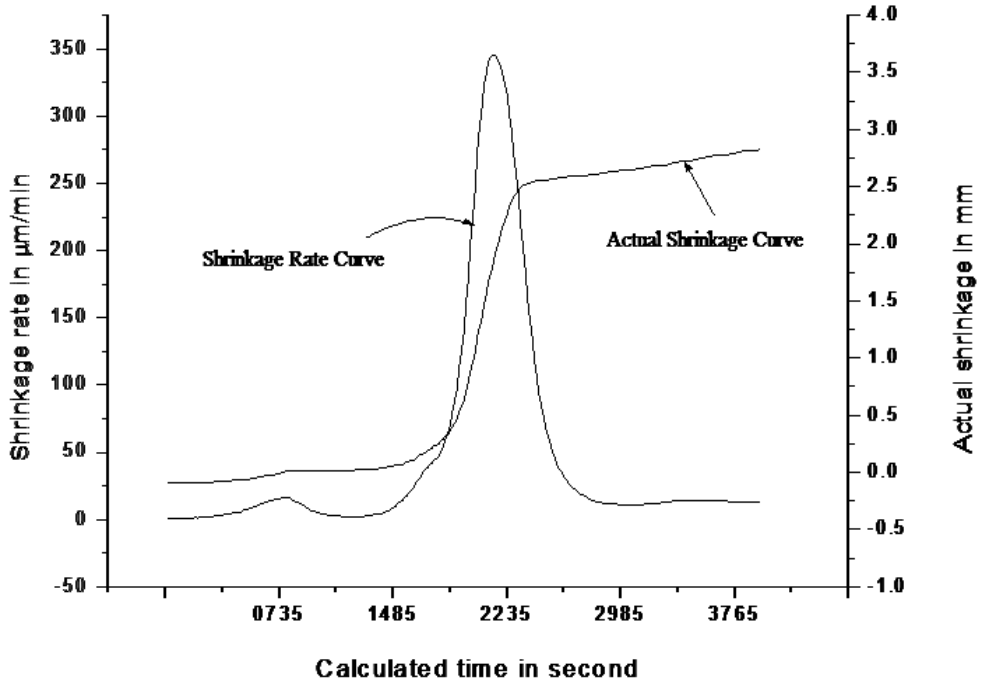

Fig. 5a. Shrinkage rate vs. temperature plot of specimen S4.

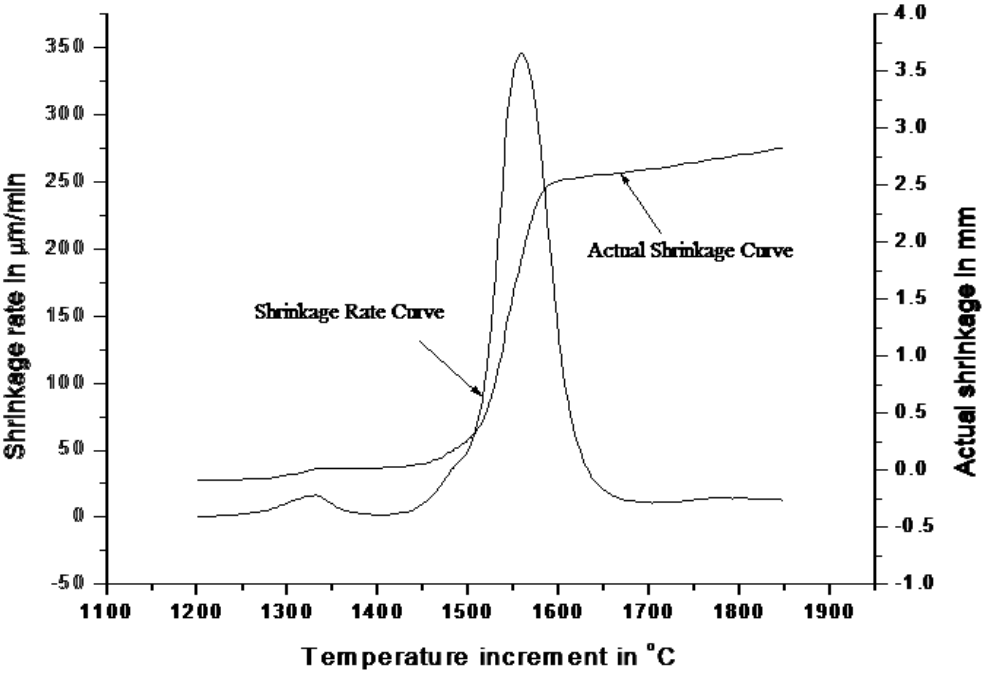

Fig. 5b. Shrinkage rate vs. time plot of specimen S4.

At 1290°C prominent peaks of α-Si_3N_4, α-Al_2O_3, and unreacted AlN were present. There was a presence of β- Si_3N_4. At 1390°C, phases of α-Si_3N_4 were predominant, whereas α-Al_2O_3 and unreacted AlN were reduced. Moreover, a new phase was developed at this temperature called DyAM ($Al_2Dy_4O_9$). During this stage, a small region of expansion was noticed on the shrinkage curve. DyAM was present for a short temperature range period and disappeared below 1450°C. For S1, at temperature 1420°C, the presence of AlN and α-Al_2O_3 were found out along with α-Si_3N_4. For S4, AlN and α-Al_2O_3 was disappeared at this temperature. Data of S2 and S3 show intermediate results. The main reaction products were between the temperature range 1450-1540°C, α-Si_3N_4 and DyAG($Al_3Dy_4O_{12}$).

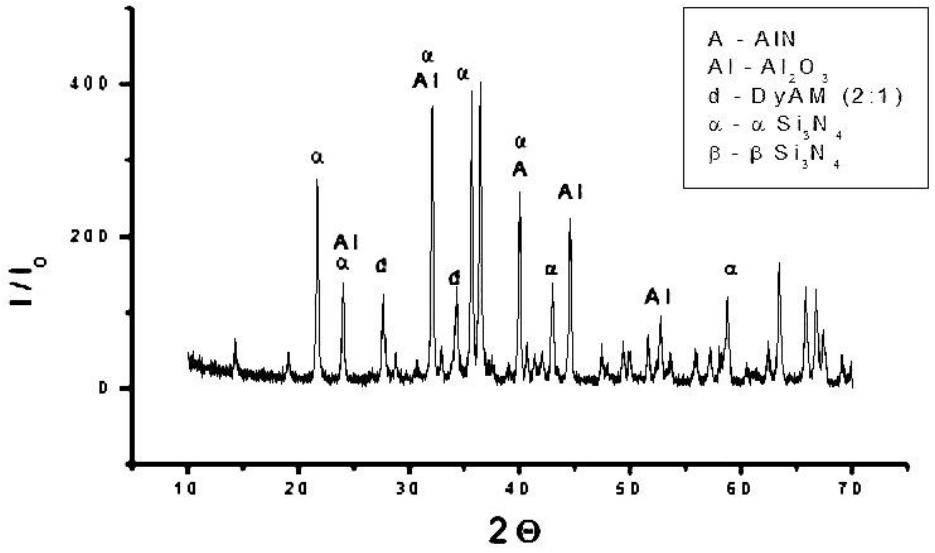

Fig. 6a. XRD analysis of sample S1 @ 1290°C.

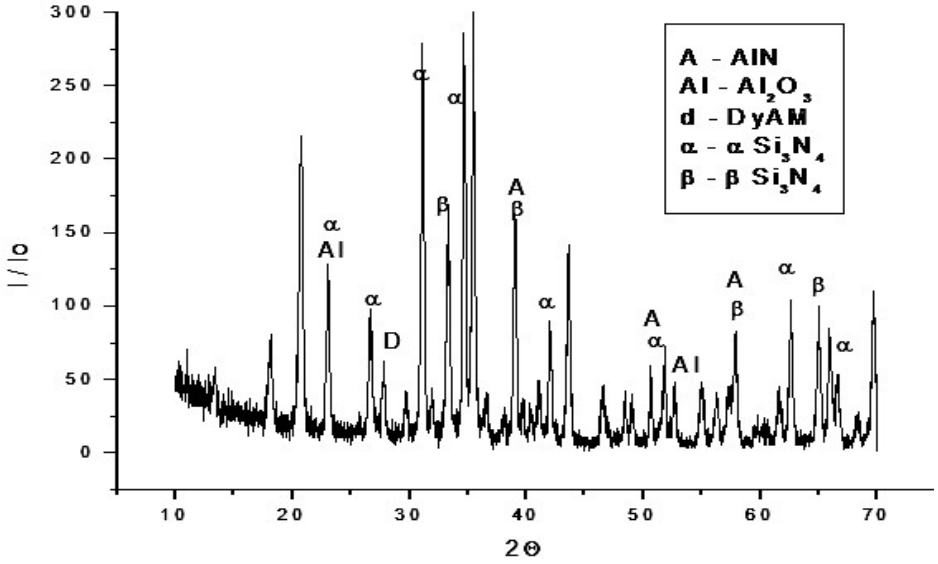

Fig. 6b. XRD analysis of sample S1 @ 1390°C.

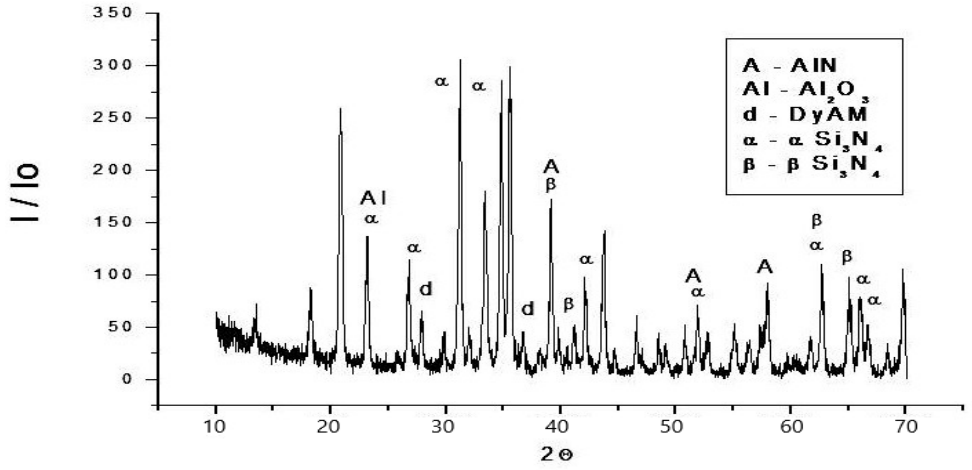

Fig. 6c. XRD analysis of sample S1 @ 1420°C.

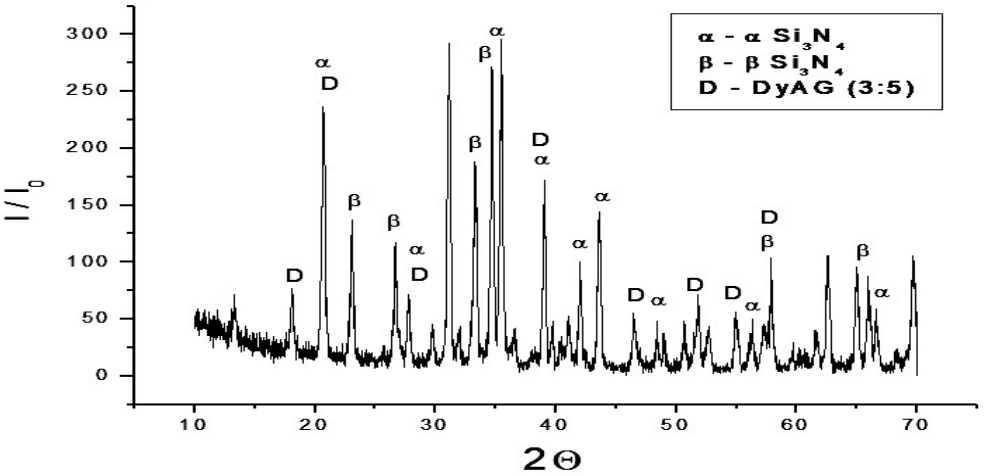

Fig. 6d. XRD analysis of sample S1 @ 1450°C.

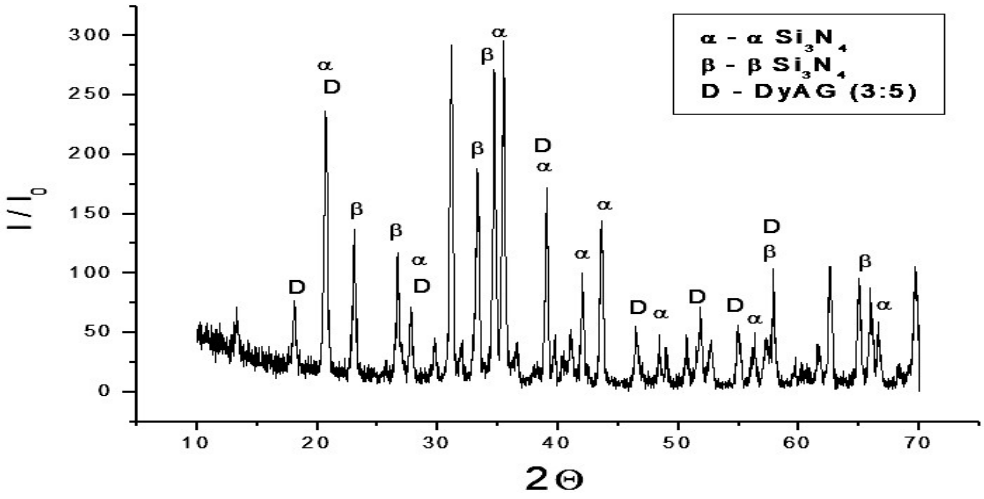

Fig. 6e. XRD analysis of sample S1 @ 1495°C.

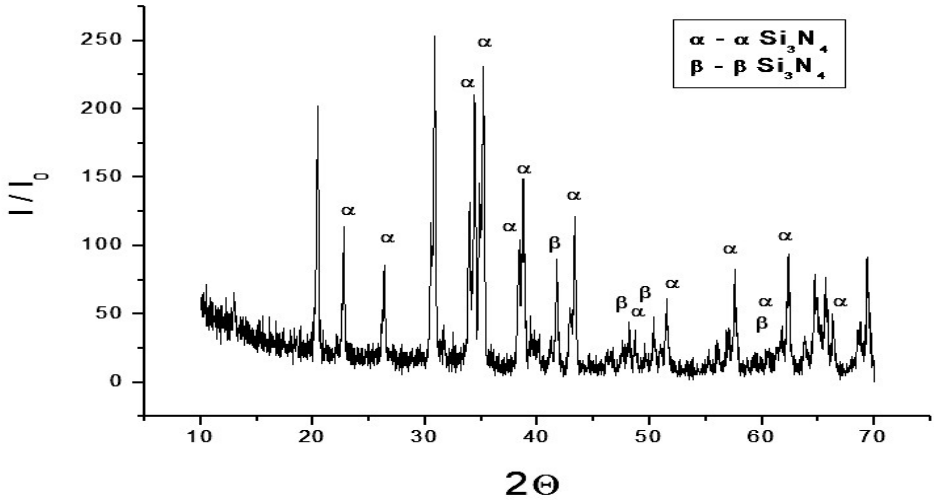

Fig. 6f. XRD analysis of sample S1 @ 1540°C.

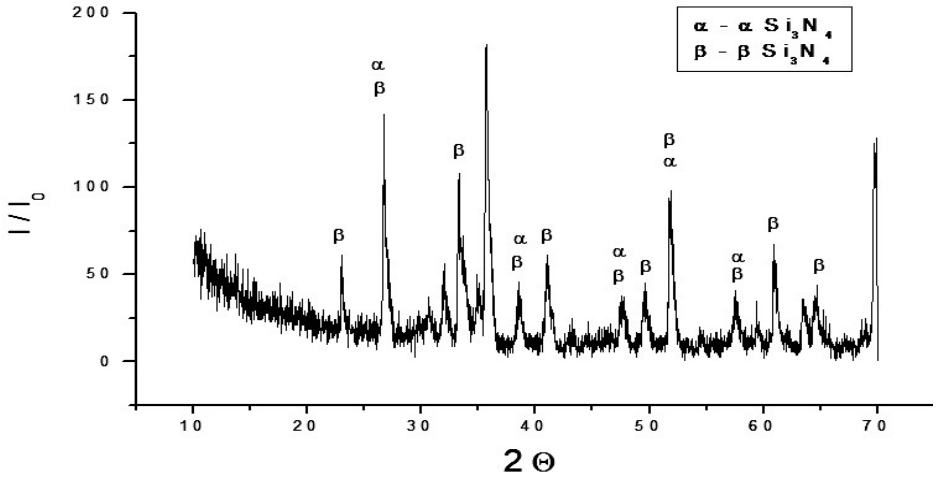

Fig. 6g. XRD analysis of sample S1 @ 1850°C.

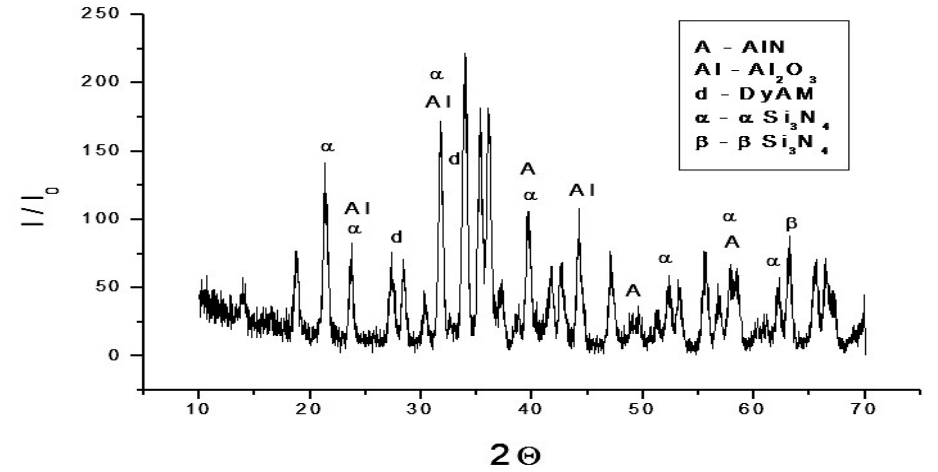

Fig. 7a. XRD analysis of sample S2 @ 1290°C.

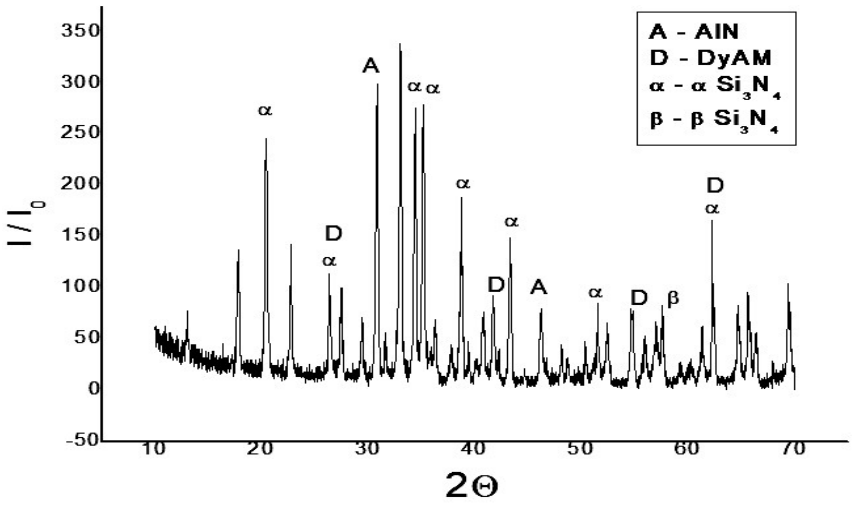

Fig.7b. XRD analysis of sample S2 @ 1390°C.

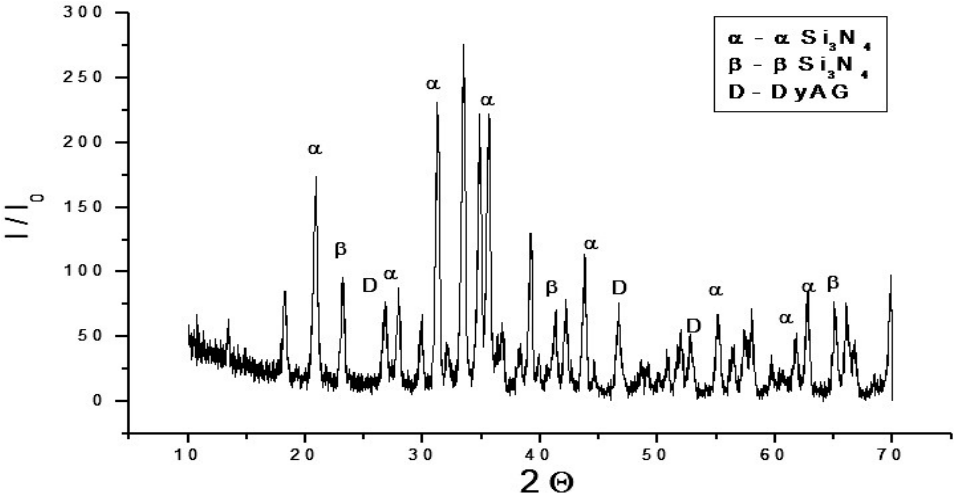

Fig. 7c. XRD analysis of sample S2 @ 1420°C.

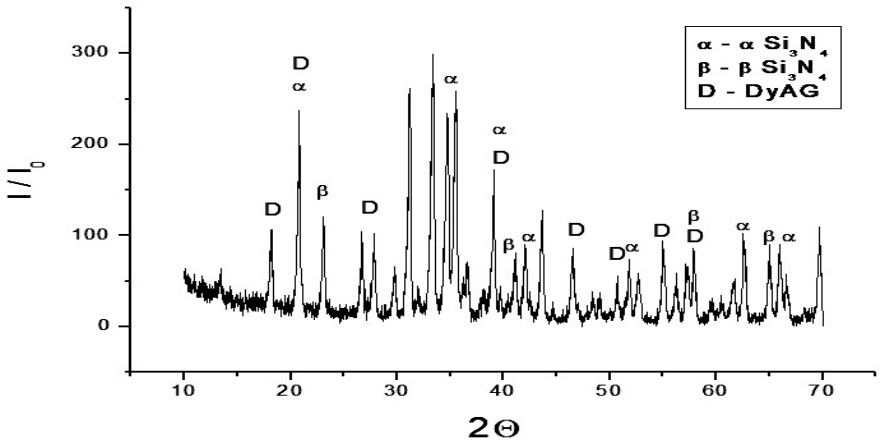

Fig. 7d. XRD analysis of sample S2 @ 1450°C.

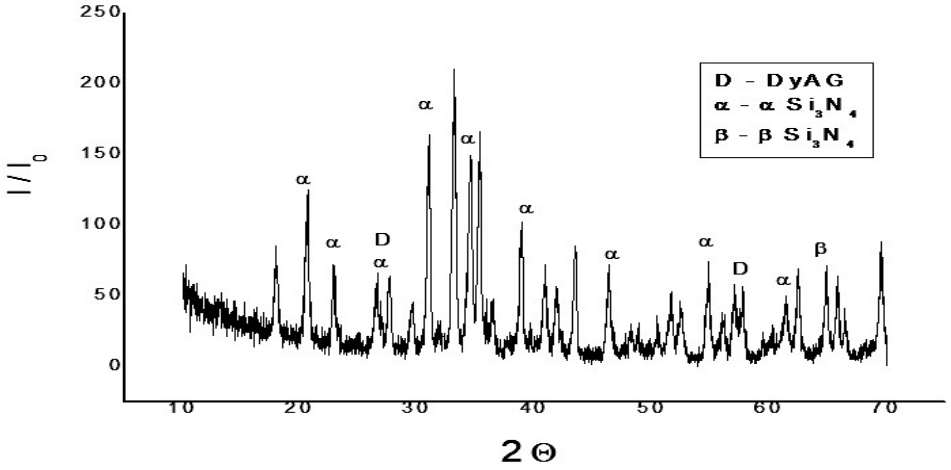

Fig. 7e. XRD analysis of sample S2 @ 1495°C.

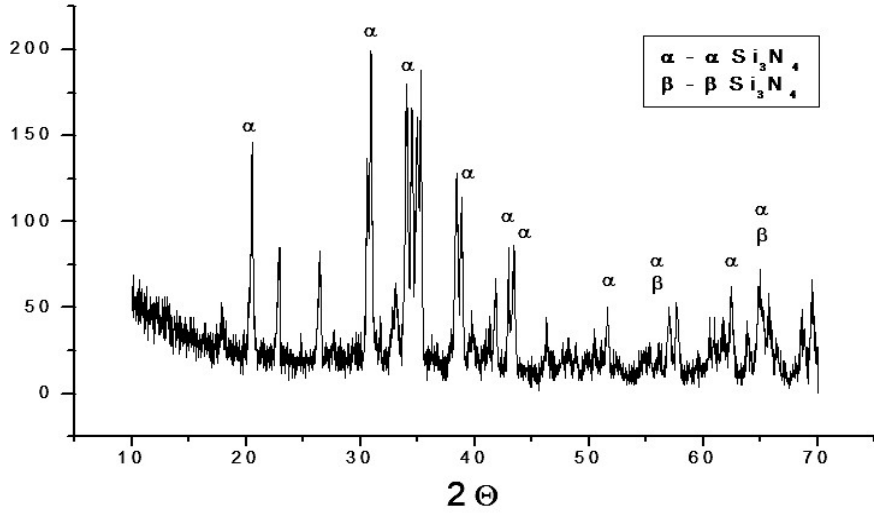

Fig. 7f. XRD analysis of sample S2 @ 1540°C.

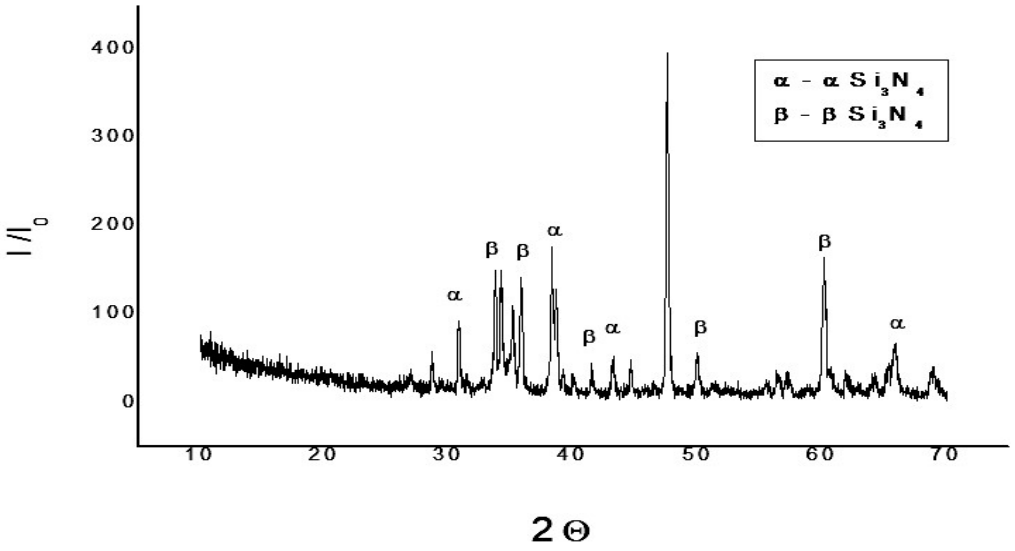

Fig.7g. XRD analysis of sample S2 @ 1850°C

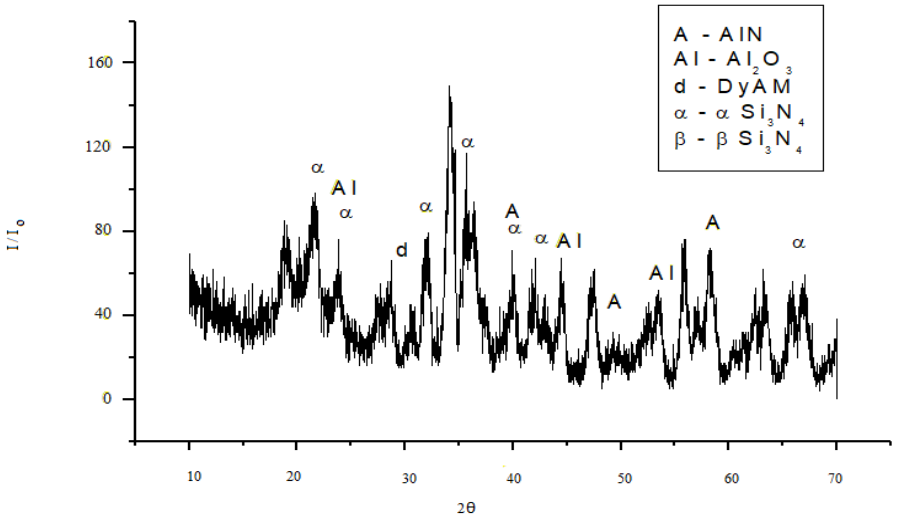

Fig. 8a. XRD analysis of sample S3 @ 1290°C.

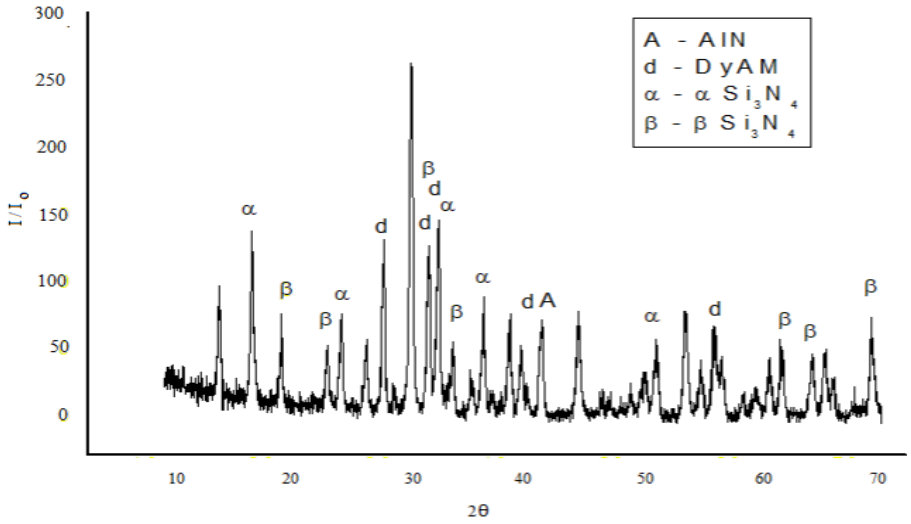

Fig. 8b. XRD analysis of sample S3 @ 1390°C.

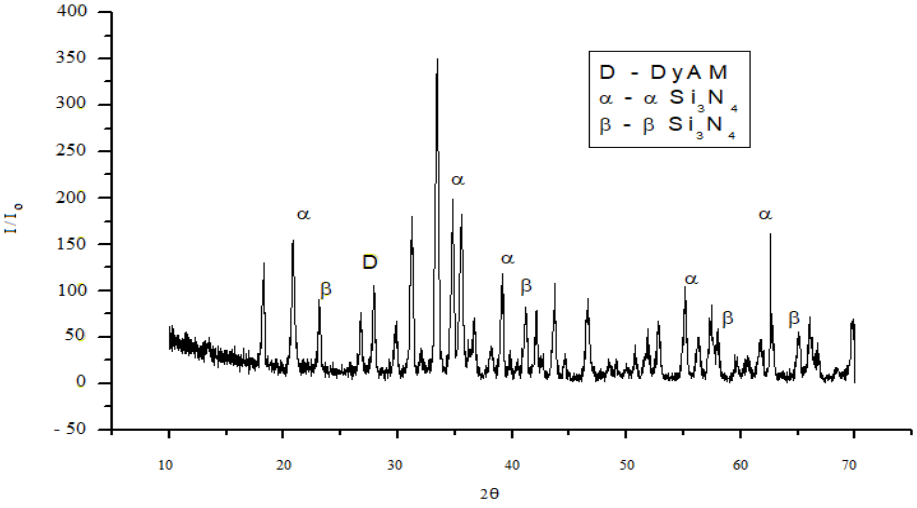

Fig. 8c. XRD analysis of sample S3@ 1420°C.

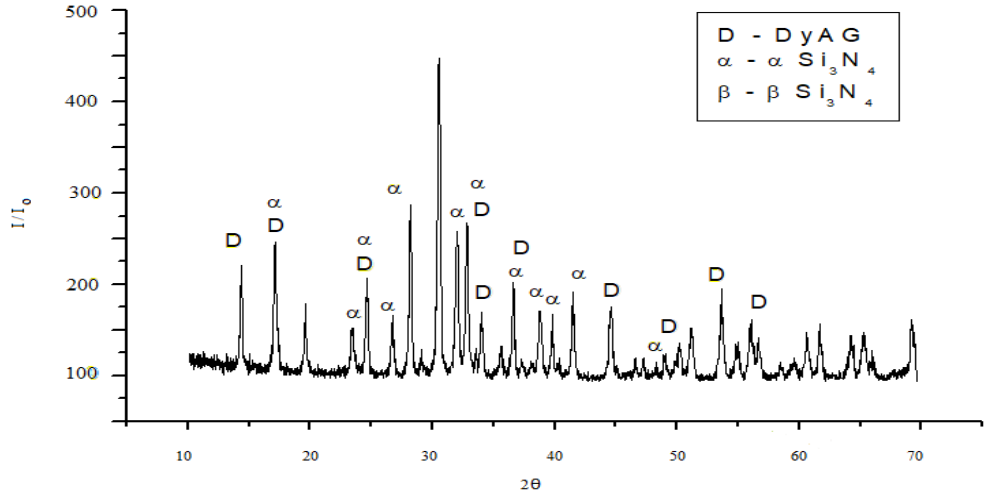

Fig. 8d. XRD analysis of sample S3@ 1450°C

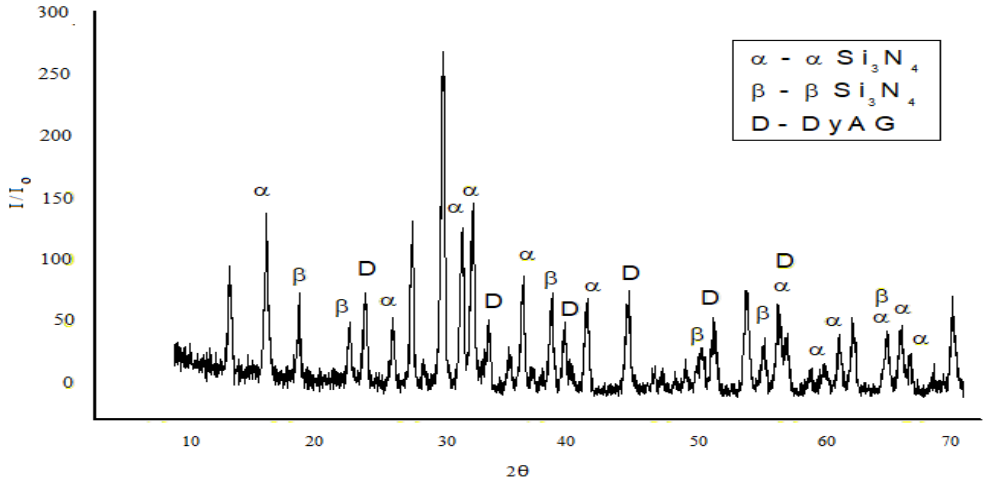

Fig. 8e. XRD analysis of sample S3@ 1495°C.

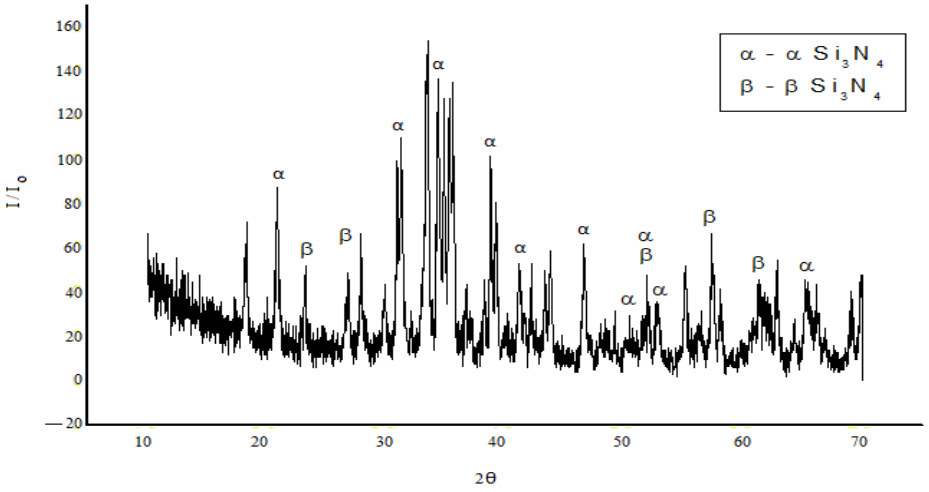

Fig. 8f. XRD analysis of sample S3@ 1540°C.

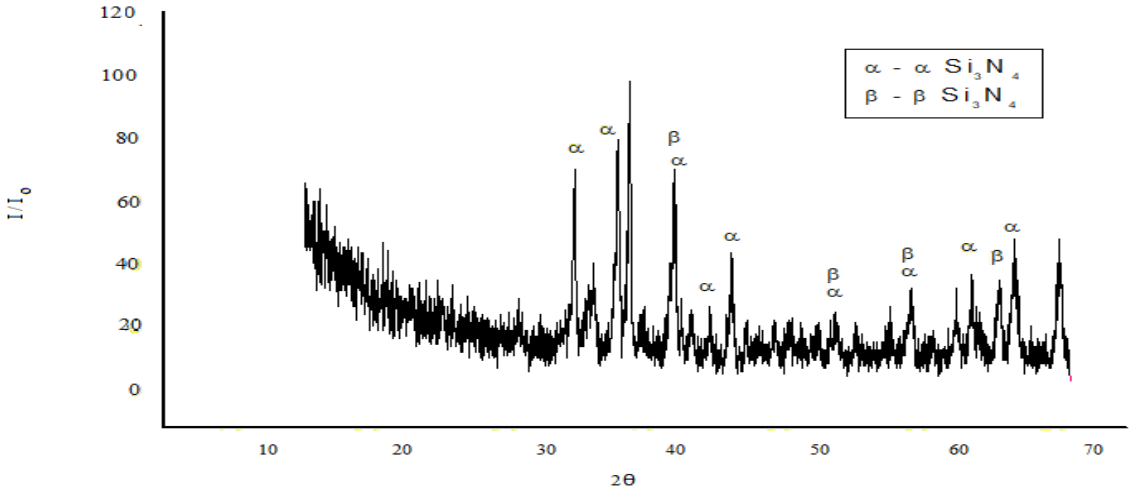

Fig. 8g. XRD analysis of sample S3@ 1850°C.

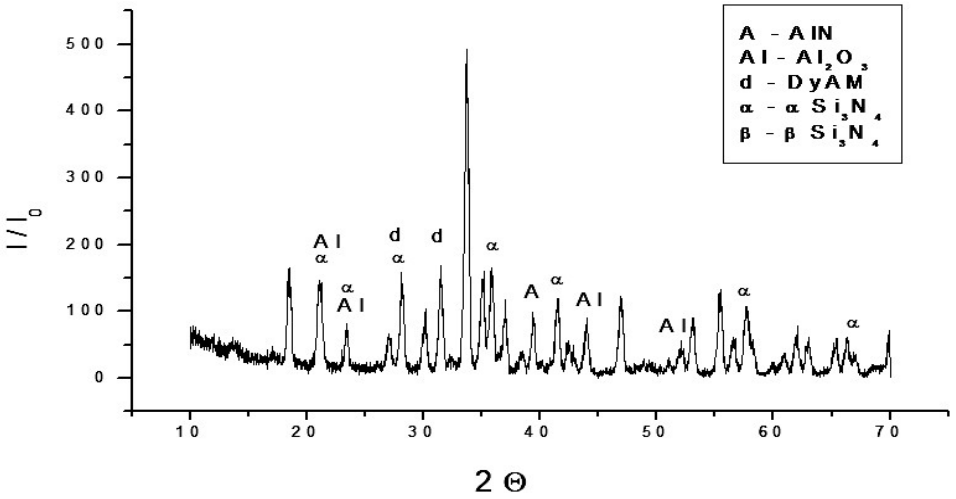

Fig. 9a. XRD analysis of sample S4@ 1290°C.

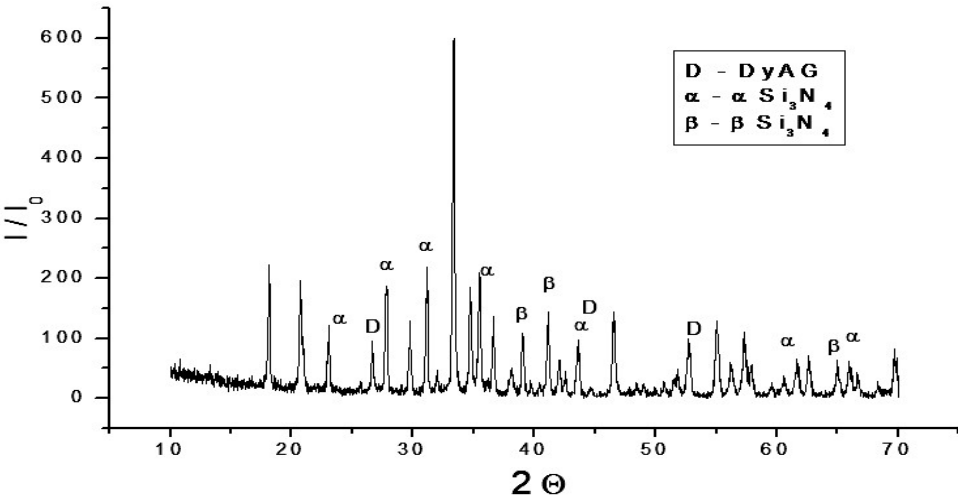

Fig. 9b. XRD analysis of sample S4@ 1390°C.

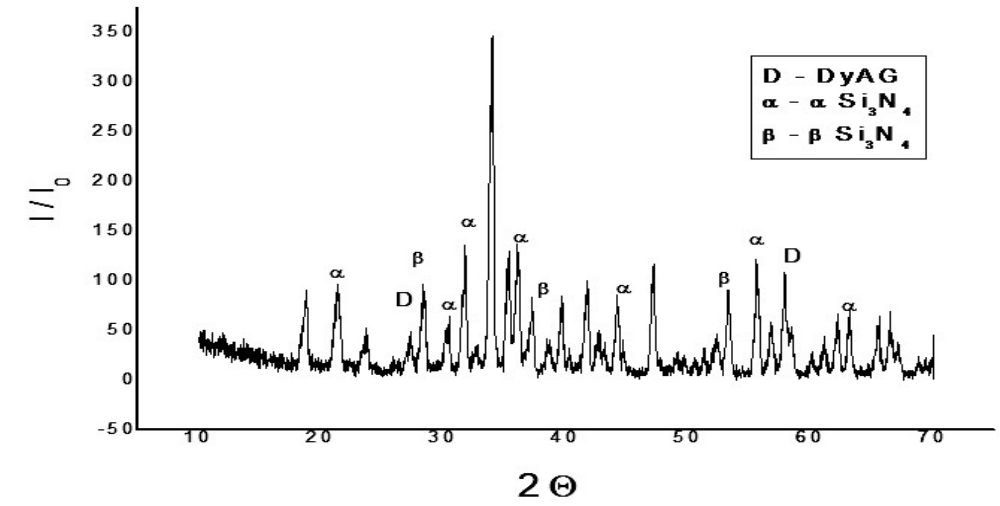

Fig. 9c. XRD analysis of sample S4@ 1420°C.

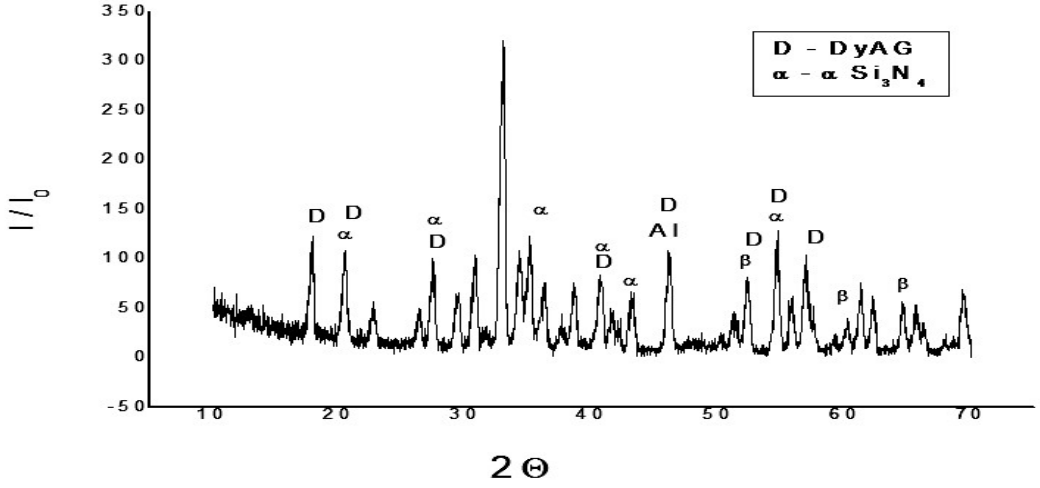

Fig. 9d. XRD analysis of sample S4@ 1450°C.

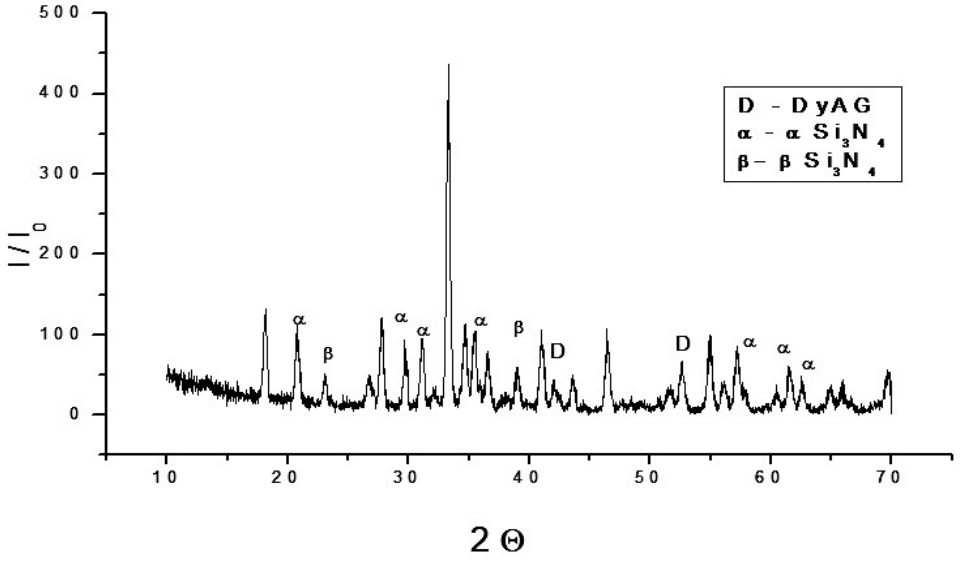

Fig. 9e. XRD analysis of sample S4@ 1495°C.

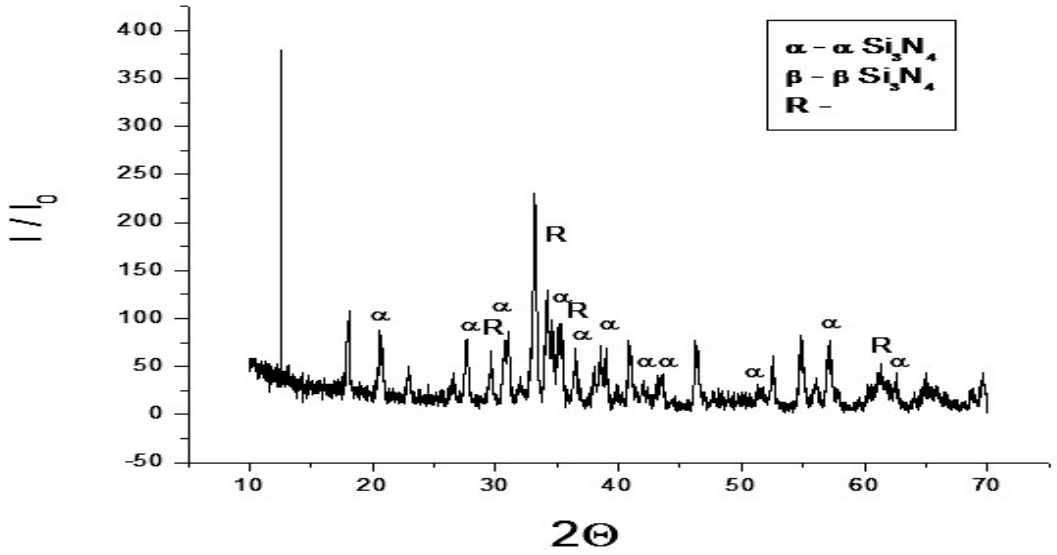

Fig. 9f. XRD analysis of sample S4@ 1540°C.

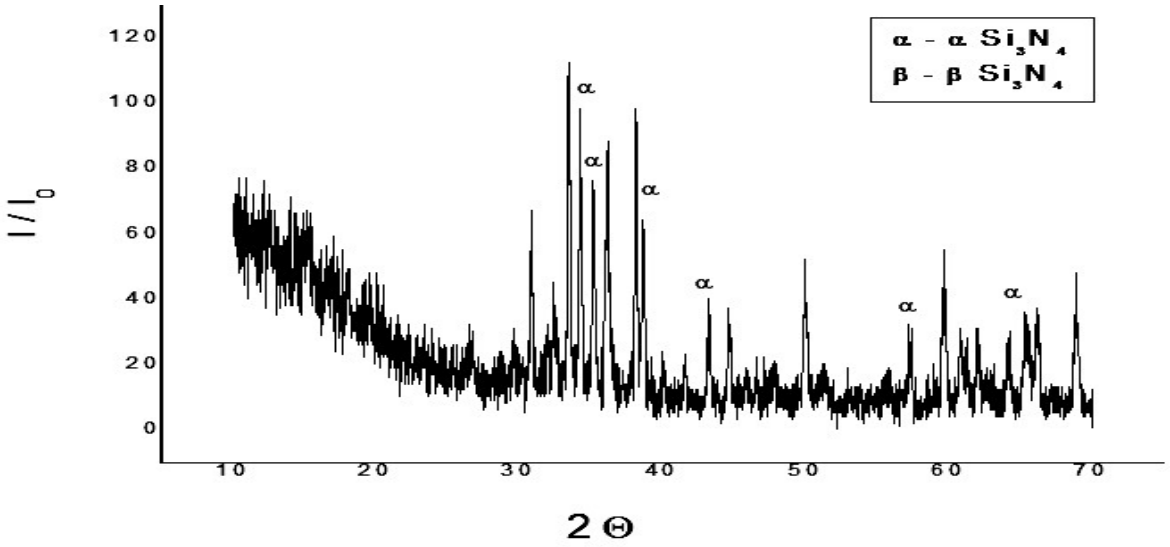

Fig. 9g. XRD analysis of sample S4@ 1850°C.

For S1 and S2, β-Si_3N_4 appeared between the temperature ranges of 1450-1495°C. At 1495°C, there was a significant shift in the XRD curve. The amount of DyAG was reduced. Major peaks of β-Si_3N_4 were merging with other phases. At 1540°C, α-Si_3N_4 and β-Si_3N_4 were present at almost 1:1 ratio. The amount of DyAG present was virtually nil, and the number of peaks has been reduced significantly. At 1850°C, the sample was fully sintered, and there were only the phases of α-Si_3N_4 and β-Si_3N_4 at a 1:1 ratio. Most of the peaks were merging. It was also noted that around 33-35°, there was a sharp peak shown in every curve, which might have been generated from the sample holder. XRD curves are shown in figures 6a-9g.

Conclusion

During the Diatometric study, it was found that S4 exhibited maximum shrinkage at the

lowest temperature, whereas S1 densified at maximum temperature with minimum shrinkage rate. At the same time, S3 and S4 exhibited a rapid rate of actual shrinkage with respect to S1 and S2. It was also found that the former pair of samples took much more time for densification than the last pair.

From the XRD analysis, it is clear that for S1 at 1420°C, unreacted AlN and α-Al_2O_3 were present within the system, whereas for S4, both the ingredients were disappeared before 1420°C. The presence of DyAM and DyAG were identified between the temperature ranges of 1420-1495°C. Thus, it was clear that the increment of additives within the sample composition enhances densification rate at a lower temperature.

Acknowledgement

The authors are grateful to Dr. S. Bandyopadhyay of Central Glass & Ceramics Research Institute, Calcutta 700 032, India for his technical help and support.

Conflict of interest

Authors declare that there is no conflict of interest.

References

Cao, G. Z., Metselaar, R. and Ziegler, G. (1992). Microstructure and Properties of Mixed α'+β'-Sialons. In: Carlsson, R., Johansson, T., Kahlman, L. (Eds). Proceedings of the Fourth International Symposium on Ceramic Materials and Components for Engines, Elsevier, New York. Pp. 188-195.

Ekstrom, T., Nygren, M., (1992). Sialon ceramics. *J. Am. Ceram. Soc.* 75 (2): 259–276.

Jack, K. H. (1976). Sialons and related nitrogen ceramics. *Mater. Sc.* 11 (6): 1135–1158.

Li, Y. W., Wang, P. L., Chen, W. W., Cheng, Y. B. and Yan, D. S. (2001). Formation behaviour, microstructure and mechanical properties of multi-cation alpha SiAlONs containing calcium and neodymium. *J. Eur. Ceram. Soc*. 21: 1273–1278.

Liu, M. and Nasser, S. N. (1998). Microstructure and boundary phases of in-situ reinforced silicon nitride. *Mater. Sci. Eng*. A254: 242–252.

Satet, R. L., Hoffmann, M. J. and Cannon, R.M. (2006). Experimental evidence of the impact of rare-earth elements on particle growth and mechanical behaviour of silicon nitride. *Materials Science Engineering*. 422A (2006): 66-76.

Shibata, N., Pennycook, S. J., Gosnell, T. R., Painter, G. S., Shelton, W. A. and Becher P. F. (2004). Observation of rare-earth segregation in silicon nitride ceramics at subnanometre dimensions. *Nature*. 428: 730- 733.

Ziegler, A., Kisielowski, C., Hoffmann, M. J. and Ritchie, R. O. (2003). Atomic resolution transmission electron microscopy of the intergranular structure of a Y_2O_3 containing silicon nitride ceramics. *J. Am. Ceram. Soc*. 86: 1777–1785.